

Mutual coupling effects in 2×2 antenna array for ground penetrating radar on multilayered soil

Marco Antonio Becerra-Pérez¹, Tanith Guerra-Huaranga¹, Maria Elisia Armas-Alvarado¹,
Mark Clemente-Arenas², Ruth Esther Rubio-Noriega¹

¹Universidad Nacional de Ingeniería, Instituto de Investigación y Capacitación de Telecomunicaciones, Lima, Perú

²CS-HF, EPIET-UNTELS, Universidad Nacional Tecnológica de Lima Sur, Lima, Peru

Article Info

Article history:

Received Nov 9, 2023

Revised Nov 24, 2023

Accepted Dec 16, 2023

Keywords:

Co-polarization

Cross-polarization

Georadar

Ground penetrating radar

Log periodic dipole array

Vivaldi

ABSTRACT

Caral stands as the Americas' oldest city, boasting a heritage spanning 5,000 years. Over time, various natural forces have woven a complex geological stratum. To gain a deeper understanding of the Caral civilization, non-intrusive exploration methodologies like ground penetrating radar (GPR) are beginning to be used. This method safeguards the integrity of ancient subterranean remains. A GPR system is in development, tailored to the [200-500] MHz range, employing a 2×2 antenna array with dual polarization. These features enhance resolution without compromising penetration depth. However, using multiple antennas within complex, multi-layered environments introduce impedance band constraints and exacerbates antenna coupling issues. This study assesses the coupling of two antenna candidates: the Vivaldi with defected ground structures (DGS) and the log periodic dipole array (LPDA). The scattering parameters show that the LPDA antenna performed better considering measured and simulated data. Cross-polarization exhibited a broader bandwidth in the LPDA antenna, evident in both simulated and measured data. Additionally, a comprehensive comparison of GPR simulations for each antenna type within an 11-level multilayer medium, with different electromagnetic properties, further highlights LPDA. This antenna boasts a 209 MHz bandwidth and a coupling better than -23 dB for the cross-polarization configuration, firmly showing its best performance.

This is an open access article under the [CC BY-SA](https://creativecommons.org/licenses/by-sa/4.0/) license.



Corresponding Author:

Ruth Esther Rubio-Noriega

Universidad Nacional de Ingeniería, Instituto de Investigación y Capacitación de Telecomunicaciones

INICTEL-UNI

San Borja, Lima, Peru

Email: rrubio@inictel-uni.edu.pe

1. INTRODUCTION

Peru boasts the distinction of being home to the oldest civilization in the Americas, Caral, with a history spanning around 5,000 years. This rich cultural heritage graces the northern region of Lima and has commanded significant scholarly attention since its initial discovery [1]. However, delving into the lives and societal structures of the Caral inhabitants requires further archaeological investigation. A focal point in this pursuit has been the search for the burial grounds [2]. Regrettably, the precise location of this cemetery remains elusive; compounding this challenge is the fact that experts posit these remnants buried at depths exceeding 10 meters.

Many techniques are available for subterranean archaeological exploration; however, the considerable age and depth of the cemetery mandate a preference for non-invasive methodologies. ground

penetrating radar (GPR) is an adequate choice, proven effective for archaeological prospecting and unobtrusive investigations [3]. GPR systems hold significant promise for delving into the cultural tapestry of Caral. However, GPR performance can vary due to the complexity of subsurface conditions, antenna configurations, signal processing techniques, and other environmental factors. Nonetheless, it is essential to acknowledge the inherent trade-off between penetration range and resolution in commercial radar systems, a challenge magnified by the crucial importance of exploration of this time-honored city in pursuit of answers.

Over the years, Caral has experienced thousands of floods, contributing to the formation of heterogeneous geological layers. The multilayered soil adds complexity to GPR exploration. Addressing this issue requires a study of wave-material interactions to characterize wave propagation mechanisms in multilayered and lossy media, which can assist in radar signal processing [4], [5]. Wave-material interactions can be characterized by means of the interaction between the GPR antennas in close proximity to one another and between the antennas and the soil [6]–[9].

In the state of the art, different antenna geometries and configurations operating at different center frequencies offer diverse results. For instance, Table 1 shows some related works on the design of antennas for GPR systems. From this parameter analysis, we draw that low center of radiating frequencies are usually associated with depth range depending on the soil type [10]. However, low centers of radiating frequencies have reduced bandwidths, affecting the effectiveness of the GPR system. For example, Vivaldi antennas in GPR applications [11]–[14] offer high gain and directivity; however, bandwidth is limited to the radiating frequency and depth range is small in most cases. Bigger depth ranges, up to 7 m [10], have been demonstrated by GPR systems with antennas with special geometries, like bowtie [10], [15] and low profile [13]; however, even further depth ranges are needed to meet the requirements of our field of application in Caral. Moreover, the complexity of the multi-layered soil could affect the working bandwidth of the antenna, making it more difficult to discern buried objects.

To obtain more information about deeply buried objects when bandwidth is narrow, the use of arrays of antennas with dual polarization has been proved a helpful tool [9]–[11]. The literature cited in Table 1 also indicates that this approach has been explored; however, most works do not analyze the wave-material interactions in terms of the analysis of coupling between antennas [10], [11]. This could lead to misreads on the working bandwidth of the antenna array and, in consequence, unidentified errors in the GPR scanning data.

To assess the matters listed above, this work studies two sets of antenna configurations for dual-polarization GPR exploration of Caral's archaeological site and analyzes the multilayered effects of the soil on the antenna configuration. We characterize and compare main georadar parameters that aid processing, such as bandwidth affected by coupling on a dual polarization antenna array, and the estimated depth range of the radar. Our work aims to contribute with a future higher penetration range, considerable bandwidth centered at a low frequency, which is needed because of Caral's antiquity and soil type.

Table 1. Works on antenna analysis for GPR systems

Antenna	Center of radiating frequency (MHz)	Bandwidth (MHz)	Gain	Depth range (m)	Dual polarization/coupling analysis	Reference
Bowtie array	660	700	-	3.5 - 7	Yes/No	Simi and Manacorda [10]
Vivaldi array	2000	3600	9 dB	0.093	Yes/No	Sun <i>et al.</i> [11]
Antipodal Vivaldi	325	75	4.4 dB	Buried object at 0.0015	No/No	Guo <i>et al.</i> [12]
Electrically narrow very low-profile antenna	450	~400	4.9 dBi	1	No/Yes	Yektakhah <i>et al.</i> [13]
Vivaldi UWB	1900	2200	-	0.12	No/No	Guan <i>et al.</i> [14]
Chevron bowties	~1.1	~30	~2 dB	0.075	No/Yes	Verre <i>et al.</i> [15]
DGS-Vivaldi	350	37.6	5.3 dB	12*†	Yes/Yes	Our work
LPDA		47	1.4 dB	5.5*‡		

*Calculated for a transmitted power of 50 W and 1 mW of minimum detectable signal in vacuum, evaluated at †249.5 MHz and ‡357.5 MHz.

2. MATERIALS AND METHODS

Let us recall the relationship between the radar system features and the antennas' parameters. Radars are based on the emission of electromagnetic waves and the recovery of the backscattered signal from the medium through which it has propagated [16]. Electromagnetic devices and components are used to generate wavefronts, which emit pulses with a certain bandwidth. Similarly, the reflected wave is recovered through another channel equipped with similar devices and components. These devices include antennas,

transmission lines, phase shifters, local oscillators among others. Particularly, antennas exhibit what is known as impedance bandwidth (BW), which can be measured through the level of impedance matching achievable at their feed port. However, in our dual-polarization georadar configuration, considering the bandwidth of one antenna alone is insufficient if it is coupled with its adjacent antenna. Thus, in cases where multiple antennas are employed in the radar systems, it is necessary to study the coupling level between them.

In this section, design and characterization methods for the antenna analysis are presented. First, we describe improved antenna designs and their fabrication process using cost-effective planar substrates. Next, we describe main georadar-related antenna characterization parameters including bandwidth, resolution, and co- and cross-polarization.

2.1. Design and fabrication methods

The ground-penetrating radar used to explore Caral requires two transmitting and two receiving antennas. On the one hand, Vivaldi antennas, also known as tapered slot antennas, are directional antennas that offer wide bandwidth and good radiation characteristics. They are particularly well-suited for applications that require broadband performance and directional radiation patterns, which is our case. Therefore, an optimized version of the Vivaldi antennas with defected ground structures (DGS) was first used for our GPR.

On the other hand, log-periodic antennas offer a broad frequency range, making them versatile for different GPR applications. They are suitable for both shallow and deep subsurface investigations. Because of this, a log-periodic antenna is the second candidate for the GPS. Our work evaluates two antenna candidates: two DGS-Vivaldi antennas that use defected ground structures, DGS-V1 and DGS-V2; two log-periodic dipole array (LPDA) antennas, LPDA-1 and LPDA-2. Table 2 describes the parameters for both antenna designs.

Table 2. Working conditions of the proposed dual polarization antenna system

Parameter	Expected value
Return loss, BW (dB)	<-10
Return loss, coupling (dB)	<-20
Min. gain (dB)	2

The design of the individual antenna elements and their simulation results in free space were previously reported [9]. Now, we report the fabrication process of our two proposed antennas on a double-faced FR4 substrate. The fabrication process consists of: i) cutting an area of 525×750 mm, ii) transferring the calculated geometry to the substrate through a paper mask, iii) coating the transferred geometry with a thin film of anti-corrosive acrylic paint, iv) etching the exposed copper from both faces using a mixture of H₂FeO₄ and H₂O₂ on a proportion of 1:1, and lastly v) cleaning the surfaces and soldering connectors. Furthermore, the orthohedron structure is composed of vinyl polychloride $\epsilon_r=4$ tubes. Also, we used ANSYS® HFSS to design each antenna and test their configurations using the orthohedron structure. Figure 1 depicts the fabricated antennas, the Vivaldi antenna in Figure 1(a) and the LPDA antenna in Figure 1(b). We measured the S-parameters in each antenna oriented towards the free space, along the Y-axis, allowing us to compare using the requirements listed in Table 2.



Figure 1. Photo of fabricated antennas (a) DGS Vivaldi antenna and (b) LPDA antenna. Each antenna has a total area of 0.4 m². For further details on design, review our previous work [9]

2.2. Characterization methods

The bandwidth of an antenna, BW, is directly linked to the radar resolution Δr through (1) [17], [18].

$$\Delta r = \frac{v}{2BW} \quad (1)$$

Where, the resolution of the radar is its ability to determine elements within its range depending on the operation frequency and bandwidth, and v is the speed of the wave in the medium. The multilayered media found in Caral could potentially affect the BW and, consequently, the resolution. Thus, a bandwidth greater than 20 MHz should be ensured over frequencies from 200 MHz to 500 MHz to meet the GPR requirements in our specific application and the processing of radar profiles.

In GPR design, the amount of power the transmitting antenna transfers to the receiving antenna is a crucial factor for determining useful information about the shape and distance of buried objects. Throughout its entire bandwidth, BW, the antenna must be capable of emitting and receiving the maximum amount of power possible while simultaneously avoiding the generation of induced currents in the metallization of the neighboring antenna; this is known as coupling. The scattering parameters, or S-matrix, can quantify coupling. Throughout our work, mutual coupling is measured using S_{ij} or S_{ji} [19]. An accepted criterion states that when these parameters are below -20 dB, coupling does not affect the transmitted signal [20]–[22]. Our proposed configuration comprises four antennas organized throughout the lateral faces of a cube. Thus, a signal from a single antenna can be interfered by the antenna at the front (co-polarization) or by the antenna at the side with a 90° rotation (cross-polarization). Table 2 describes the minimum working conditions for the coupling analysis of our proposed dual polarized antenna system for GPR. The results sections will use the same parameters for evaluation and comparison.

3. RESULTS OF THE ANTENNA ANALYSIS IN FREE SPACE

The antenna system analysis involves comparing the measurement and simulation results of two types of antennas, DGS-V and LPDA. On the one hand, the reflection coefficient S_{ii} and transmission coefficient S_{ij} of both antennas are compared. Simulation results were obtained using ANSYS® HFSS software on an INTEL Core i9 processor with RAM of 128 GB computer and a server with 32 cores and 256 GB RAM. On the other hand, measured data was acquired using a vector network analyzer N9960A FieldFox Handheld VNA.

3.1. Single antenna characterization

The first step in measuring antennas is to evaluate their return losses in free space. First, it is necessary to measure each antenna separately. Figure 2 compares the fabricated and simulated DGS Vivaldi antennas, namely DGS-V1 and DGS-V2. It is worth noting that we measured minor errors in manufacturing, but they were found to be less than 3% and contributed to the bandwidth and peak variations between DGS-V1 and DGS-V2. According to the return loss, S_{11} , depicted in Figure 2, the DGS-V1 antenna resonates at 240.5 MHz with a bandwidth of 47 MHz and an amplitude of -42.7 dB. In contrast, the DGS-V2 antenna radiates at 237.5 MHz with a bandwidth of 40 MHz and an amplitude of -20.895 dB. However, both radiation frequency measurements differed from the simulated results, with a relative error of 1.23% and 2.46%, respectively.

The return loss of the LPDA antennas, fabricated and simulated, is depicted in Figure 3. LPDA-1 and LPDA-2 resonate at different frequencies, with LPDA-1 resonating at 272 MHz, 358.9 MHz, and 442.9 MHz, and LPDA-2 resonating at 263 MHz, 352.9 MHz, and 438.5 MHz. The measured resonant peaks differ from the simulation by less than 2.8%. The simulated results suggest that the LPDA antenna has an ultra-wideband at 240.4 MHz. However, the measured results reveal three separate bandwidths, each with different widths: approximately 37.7 MHz, 60 MHz, and 65.1 MHz. These deviations occur due to slight variations in the dimensions of the dipoles, which impact the magnitude of the S_{11} , especially at high frequencies.

3.2. Coupling analysis

As mentioned, mutual coupling can be obtained through the parameter dB (S_{ij}), where i and j are the port numbers. These parameters should be lower than -20 dB to avoid significant interference between two nearby antennas. Two configurations are analyzed using a set of two DGS-Vivaldi and two LPDA antennas. First, we measured co-polarization using two antennas, one in front of the other at a distance of 800 mm. We measured cross-polarization using two antennas, one beside the other. To conduct parameter measurements under optimal conditions for our study, we positioned the antenna array to point directly at the zenith (z) on top of a table constructed from low-permittivity polystyrene material. The wavelength and antenna

dimensions need large anechoic chambers for precise measurements; such chambers are unavailable in our country and are scarce on the continent.

Figures 4 and 5 show the co- and cross-polarization analysis of the DGS-Vivaldi antennas, respectively. From Figure 4, we conclude that there is no interference between co-polarized antennas, while in Figure 5, we can see a peak around 275 MHz over the -20 dB mark outside the bandwidth of a single DGS-Vivaldi antenna, which suggests that at least the working BW of DGS-V1 and DGS-V2 are free of interference. We suggest that the differences between measured and simulated results occur because of the measurement configuration. As we lack an anechoic chamber in the frequency regime that the GPR system requires, the polystyrene bricks used to accommodate the antenna setup (inset in Figures 4 and 5) alter the radiation pattern directed towards the free space. In this setup, the considerable amplitude of the DGS-Vivaldi antenna backward lobe causes impedance alterations at the input dependent on the frequency. While the results are not precisely similar, the measured mutual coupling is always $\text{dB}(S_{12}) < -20\text{dB}$.

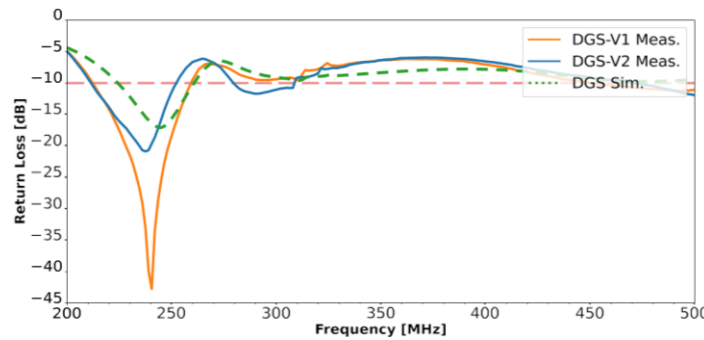


Figure 2. Return loss $\text{dB}(S_{11})$ of the single DGS-Vivaldi antennas measured and simulated in free space

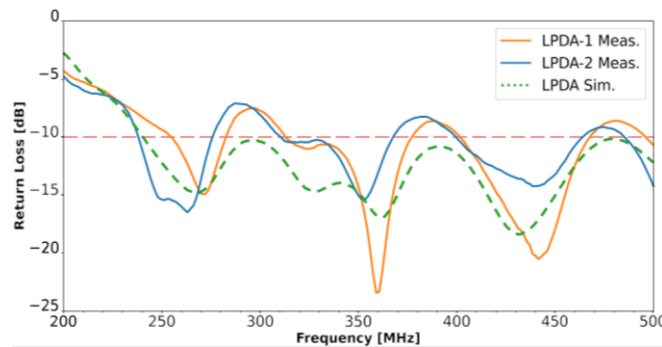


Figure 3. Return loss $\text{dB}(S_{11})$ of the single LPDA antennas measured and simulated in free space

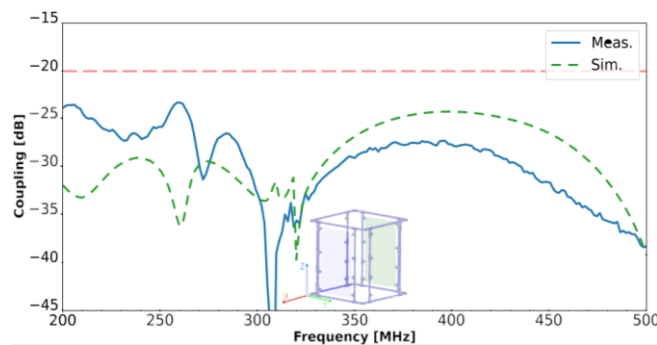


Figure 4. Co-polarization mutual coupling $\text{dB}(S_{12})$ of a DGS-Vivaldi antenna. The inset shows the configuration of the antennas on opposed faces of the orthohedron (co-polarized) for simulated and measured antenna arrays

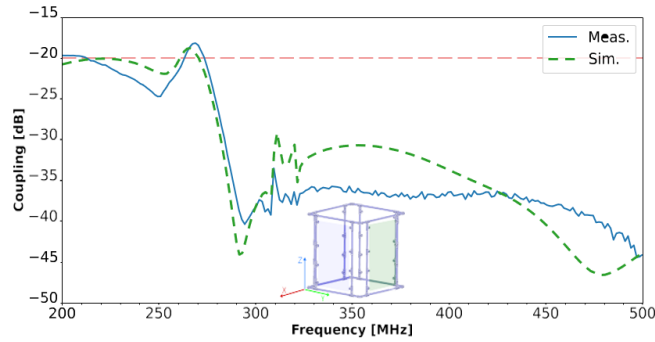


Figure 5. Cross-polarization mutual coupling $dB(S_{12})$ of a DGS-Vivaldi antenna. The inset shows the configuration of the antennas on consecutive faces of the orthohedron (cross-polarized) for simulated and measured antenna arrays

The measurements of the LPDA antenna in the two previous configurations provided considerably closer results. The co- and cross-polarization coupling outcomes of the LPDA antennas, as presented in Figures 6 and 7, further supported this. From the figures, it was evident that there was no coupling between the antennas, as indicated by $dB(S_{12}) < -20dB$. Notably, Figure 7 illustrated a band ranging from 210 to 240 MHz, which was in proximity to -20 dB. This outcome was consistent with the operational parameters specified in Table 2.

The results demonstrate a significantly closer correspondence between measurement and simulation when compared to the DGS-Vivaldi antenna. This favorable outcome serves as an initial criterion for selecting the LPDA antenna. Besides exhibiting the required mutual coupling as per the specifications, it is also evident that the measurement conditions have not significantly impacted the outcome.

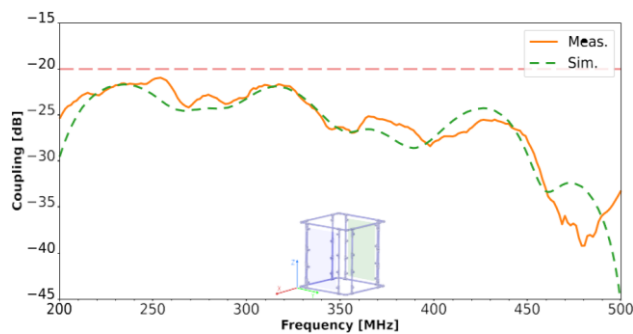


Figure 6. Co-polarization mutual coupling $dB(S_{12})$ of a LPDA antenna. The inset shows the configuration of the antennas on opposed faces of the orthohedron (co-polarized) for simulated and measured antenna arrays

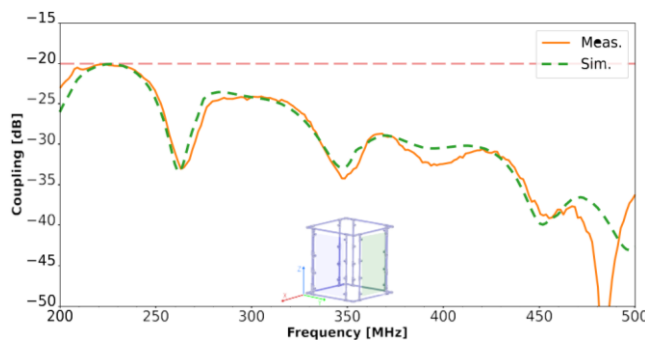


Figure 7. Cross-polarization mutual coupling $dB(S_{12})$ of a LPDA antenna. The inset shows the configuration of the antennas on consecutive faces of the orthohedron (cross-polarized) for simulated and measured antenna arrays

4. RESULTS OF THE ANTENNA ANALYSIS ON A MULTILAYERED SOIL

GPR is a geophysical technique that uses radar pulses to image subsurface features. However, multilayered soil can significantly affect the interpretation of GPR parameters, which can impact the data collected. The Caral archaeological site, for example, has multiple layers of sediment in its subsurface, with as many as 11 distinguishable strata. While the arrangement of these layers has been confirmed at specific points within the area, it would be impractical to excavate at multiple points to establish a typical subsurface profile. As a result, the distribution outlined in Table 3 and illustrated in Figure 8 is the most accurate representation of the subsurface composition within the area targeted for GPR analysis. To accurately model the multilayered soil, it is viewed as a heterogeneous media composed of eleven layers, with each layer's relative permittivity (ϵ_r), electrical conductivity, and thickness listed in Table 3.

Table 3. List of multilayered soil properties used in the analysis setup

Layer	Thickness (mm)	Colour	ϵ_r	Conductivity (siemens/m)
Air	1570	Light blue	1	0
M1	600	Purple	6	0.0001
M2	400	Yellow	15	0.0001
M3	600	Blue	16	0.0002
M4	550	Pink	17	0.00025
M5	1600	Forest	3	0.0001
M6	650	Magenta	18	0.00045
M7	400	Orange	19	0.0005
M8	1750	Petal	13	0.0012
M9	450	Gray	20	0.00065
M10	1000	Cream	10	0.001
M11	230	Brown	22	0.0007

Assessing the return losses and mutual coupling of antennas when operating in the presence of a subsurface profile is critical. To achieve this, we simulated two sets of antennae—one with DGS-Vivaldi antennas and the other with LPDA antennas, pointing towards a multilayered soil as presented in Figure 8. The setup comprised an array of antennas arranged along the lateral faces of an orthohedron, radiating towards eleven layers of media chiefly composed of gravel and sand. To simulate an infinite domain, we enforced boundary conditions using perfectly matched layers (PML) along the six boundaries, $+\hat{x}$, $-\hat{x}$, $+\hat{y}$, $-\hat{y}$, $+\hat{z}$, $-\hat{z}$.

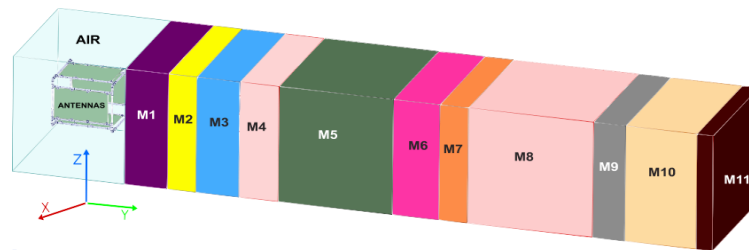


Figure 8. Antennas pointing towards the multilayered soil. Material properties are listed in Table 3

The results from the measurements of the two sets of our four antennas in free space are presented for comparison purposes. These findings are then compared with the simulation results of two sets of four identical antennas, this time considering the presence of a multi-layered ground. Figure 9 depicts the return loss comparison of the antenna configurations. The S_{11} parameter was simulated and measured in free space (green dashed line and blue solid line respectively), and multilayer pointing towards the soil (orange solid line), as shown in the inset in Figures 9(a) and 9(b). The measurements confirm the presence of three operating bandwidths that could comply with the requirements of the proposed GPR parameters. These bandwidths are (i) $BW=37.6$ MHz at a center frequency of 249.5 MHz for the DGS-Vivaldi antennas (depicted in yellow shadow in Figure 9(a)), (ii) $BW=47$ MHz at 249.5 MHz (orange shadow in Figure 9(b)), and (iii) $BW=206$ MHz at 352.5 MHz (blue shadow). Figure 9(a) indicates that all models based on DGS - Vivaldi antennas have an approximate bandwidth of 38 MHz around a center frequency of 243.5 MHz. The relative error between the three bandwidths is 0.03.

The results depicted in Figure 9(b) show three significant resonances at 252.5 MHz, 357.5 MHz and 423 MHz. Numerical results suggest that the second and third resonances conform to a single bandwidth from 310 MHz to 500 MHz; however, the measurements in free space showed a high return loss at 380 MHz. We believe this is due to the sensitivity of the LPDA antenna to minor fabrication errors [23]. A map of the mean percent dimensional error of the fabricated antennas is shown in Figure 10. Note in the color scale of this figure, that a maximum mean error of 2.7% was detected in the main feed of the LPDA antennas. The mean error in DGS-Vivaldi antennas is 1.98% and 1.20% for the LPDA antennas, with a standard deviation of 0.67 and 0.88, respectively. It is important to note that, regarding the multilayer simulation studies of the LPDA antenna array in Figure 9(b), the bandwidth at 250 MHz of the antenna array pointing towards a multilayered soil was reduced to around 54% of its original value in free-space. This is a significant drawback compared to the DGS Vivaldi antenna array, with only 3% of its original bandwidth affected by the multilayered soil as shown in Figure 9(a). However, the LPDA antenna array has another working bandwidth which is colored blue in Figure 9(b), this bandwidth does not get significantly affected by the multilayered soil exposition.

Figure 9(b) shows that all three models based on LPDA antennas have an approximate bandwidth of 35 MHz around a center frequency of 260 MHz. The relative error between the three bandwidths is 0.0317. Similarly, coupling is essential in determining the effective bandwidth. For this reason, the same cases as those analyzed for return losses are compared. Figure 11 depicts the calculated coupling between the GPR antennas, Figure 11(a) shows the co-polarization analysis and Figure 11(b) shows the co-polarization analysis. The magnitude of the cross-polarization of DGS-Vivaldi antennas as shown in Figure 11(a) in free space and on top of a multilayered soil do not approach the -20 dB mark inside the working bandwidth (yellow highlight). The estimated amplitude of cross-polarized LPDA antennas is also free of coupling at the two working bandwidths (yellow and blue highlights) in multilayer and free-space simulations.

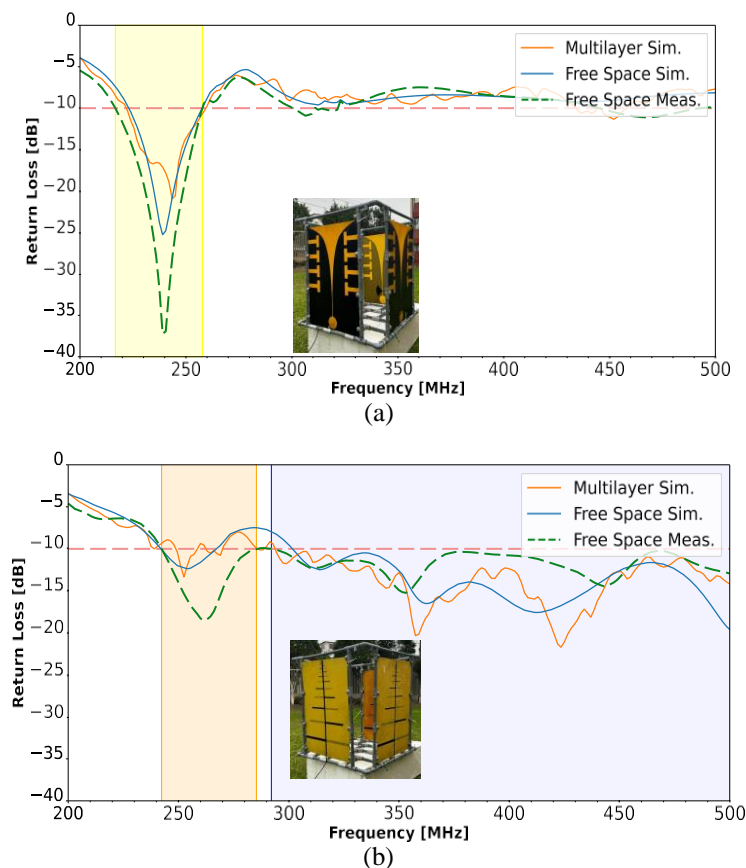


Figure 9. Return loss in dB (S_{11}) of (a) DGS – Vivaldi and (b) LPDA antenna configurations evaluated in free space and on a multilayered soil. Simulated and measured data in free space (green dashed line and blue solid line respectively), and antennas simulated considering multilayer pointing towards the soil (orange solid line). Yellow, orange and blue shadowed regions depict working radiation bands. Insets show photos of the experimental configuration for measurements

Figure 11(b) shows that coupling of DGS-Vivaldi antennas in co-polarization is negligible in both cases, free space and multilayer. LPDA antenna configuration in free space is also below the -20 dB threshold. However, the same configuration evaluated in the multilayered soil suggests possible interference at ~ 348 MHz in the blue bandwidth and at ~ 235 MHz and ~ 250 MHz in the yellow bandwidth. Moreover, none of the peaks exceed -17.5 dB. If measurements support these predictions, the coupling can still be considered insignificant.

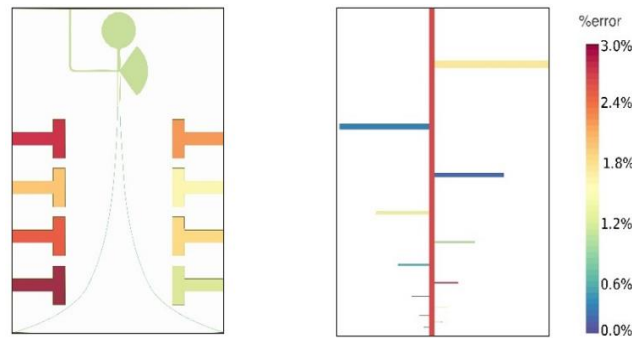


Figure 10. Geometrical distribution of mean percent dimensional error between the simulated and measured DGS-Vivaldi (left) and LPDA (right) antenna surfaces

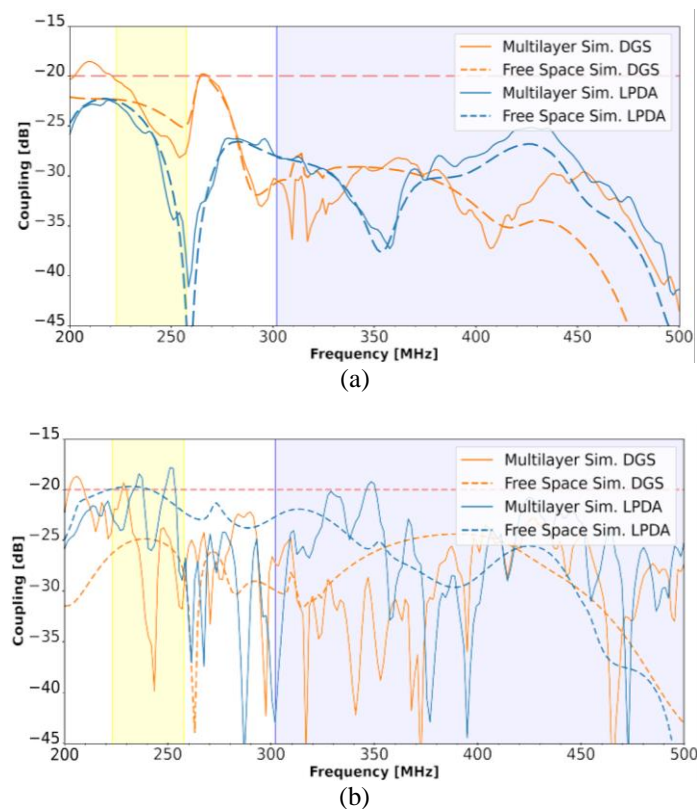


Figure 11. Mutual coupling results of 4-antenna configuration in free space and on a multilayered soil. S_{12} parameter is evaluated in (a) cross- and (b) co-polarization. Yellow and blue shadowed regions depict working radiation bands

To summarize these results, Table 4 compares the requirements for the GPR application of our antenna configurations in the archaeological city of Caral. The LPDA and DGS Vivaldi antenna configurations have approximately the same working bandwidth at 249.5 MHz. Furthermore, the LPDA

antenna configuration has an additional ultra-wide bandwidth of 207 MHz at 357.5 MHz. Both comply with the resolution and penetration range, considering the transmitted power of 50 W, which is a mean value used by recent GPR applications [24], [25] and minimum detectable signal in vacuum of 0.1 dBm, which is a typical value for software-defined radio equipment [26], [27] available in our lab. Note that the penetration range of 12 m is enough to look for archaeological remainings in spite of the previously calculated effects of the multi-layered soil.

Table 4. Comparison between the behaviour of the two antenna configurations for dual-polarization GPR exploration

Parameters	DGS vivaldi		LPDA	
	Free space	Multi-layer	Free space	Multi-layer
Bandwidth (MHz) @ 249.5 MHz	41	37.6	43	47
Bandwidth (MHz) @ 357.5 MHz	-	-	207.8	206
Co – polarization coupling ≥ -20 dB	No	Minor	No	Minor
Cross – polarization coupling ≥ -20 dB	No	Minor	No	No
Resolution (m) @ $\epsilon_{\min} = 3$	-	2.25	-	2.22
Resolution (m) @ $\epsilon_{\max} = 22$	-	0.83	-	0.82
Depth range (m)	-	12	-	5.5

While the LPDA antenna configuration delivers better results than the DGS Vivaldi within the operating range of 242 MHz to 285 MHz, it is worth noting that an even more favorable performance is observed in a different frequency range. Specifically, the array demonstrates superior performance between 292 MHz and 500 MHz, encompassing a bandwidth of 207 MHz. Within this range, the gain falls within the 3.5 dB to 7.59 dB range, and the difference between co and cross-polarization exceeds 15 dB. Consequently, both configurations yield satisfactory results for frequencies below 300 MHz, whereas the LPDA array exclusively excels for frequencies exceeding 290 MHz.

5. CONCLUSION

Using multiple antennas in the context of ground-penetrating radars in soil with multiple layers has allowed us to highlight significant differences between the DGS-Vivaldi and LPDA antenna designs. Although both antennas share similar dimensions that meet the mandatory design requirements for the exploration zone, performing an antenna parameter comparison was essential to assess the effects of the multi-layered soil of an archaeological zone such as Caral. Bandwidth and coupling between antenna arrays in different configurations were evaluated in free-space and upon the presence of a multi-layered soil, which conveyed significant bandwidth affectation of the four-antenna systems. We draw from the simulated and measured data that LPDA antennas emerge as a generally more robust option. Their results demonstrate greater consistency across changes in configuration and measurement conditions. We also conclude that formal studies on the effects of multilayered soil on dual-polarized antenna configurations is crucial for the estimation of the bandwidth and coupling.

ACKNOWLEDGMENT

The authors would like to acknowledge funding support from CONCYTEC-PROCIENCIA [contract number 140-2017-FONDECYT].

REFERENCES

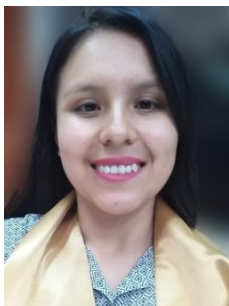
- [1] R. S. Solis, "America's first city? the case of late archaic Caral," in *Andean Archaeology III*, Boston, MA: Springer US, 2006, pp. 28–66.
- [2] C. T. Winter and D. S. Sutil, "Theoretical perspectives for an interpretive archaeology of death (*in Spanish: perspectivas teóricas para una arqueología interpretativa de la muerte*)," *Anales de la Universidad de Chile*, vol. 0, no. 6, Aug. 2010, doi: 10.5354/0365-7779.1997.3133.
- [3] M. Lohmus, M. Malve, J. Plado, and A. Tsugai, "Archaeological research at veibri: a late mesolithic cemetery anda mass grave from the 13th century AD," *Archaeological Fieldwork in Estonia*, pp. 89–102, 2010.
- [4] C. Strobbia and G. Cassiani, "Multilayer ground-penetrating radar guided waves in shallow soil layers for estimating soil water content," *Geophysics*, vol. 72, no. 4, pp. J17–J29, Jul. 2007, doi: 10.1190/1.2716374.

- [5] J. Churio, A. Ochoa, and Z. Morantes, "Simulation of electromagnetic wave propagation in enclosed environments using 3D PML-type absorbing boundaries in Spanish: simulación de la propagación de ondas electromagnéticas en ambientes cerrados utilizando fronteras absorbentes tipo PML en 3D)," *Télématique*, vol. 9, no. 1, pp. 76–97, 2010.
- [6] W. Zhang, A. Hoorfar, and Q. An, "Three-dimensional ground-penetrating radar imaging through multilayered subsurface," *Radio Science*, vol. 54, no. 8, pp. 728–737, Aug. 2019, doi: 10.1029/2018RS006605.
- [7] M. Africano, J. O. Vargas, R. Adriano, D. B. Oliveira, and A. C. Lisboa, "Ground-penetrating radar antenna design for homogeneous and low-loss dielectric multilayer media," *Journal of Microwaves, Optoelectronics and Electromagnetic Applications*, vol. 19, no. 2, pp. 137–151, Jun. 2020, doi: 10.1590/2179-10742020v19i2810.
- [8] F. Sagnard, "Design of a compact ultra-wide band bow-tie slot antenna system for the evaluation of structural changes in civil engineering works," *Progress In Electromagnetics Research B*, vol. 58, no. 58, pp. 181–191, 2014, doi: 10.2528/PIERB14013004.
- [9] T. Guerra-Huaranga, R. Rubio-Noriega, and M. Clemente-Arenas, "Comparative analysis of three types of VHF/UHF antennas for GPR array," May 2020, doi: 10.1109/LAMC50424.2021.9602503.
- [10] A. Simi and G. Manacorda, "The NeTTUN project: design of a GPR antenna for a TBM," in *Proceedings of 2016 16th International Conference of Ground Penetrating Radar, GPR 2016*, Jun. 2016, pp. 1–6, doi: 10.1109/ICGPR.2016.7572648.
- [11] H. H. Sun, Y. H. Lee, W. Luo, A. C. Yucel, L. F. Ow, and M. L. M. Yusof, "Compact dual-polarized vivaldi antenna with high gain and high polarization purity for GPR applications," *Sensors (Switzerland)*, vol. 21, no. 2, p. 503, Jan. 2021, doi: 10.3390/s21020503.
- [12] J. Guo, J. Tong, Q. Zhao, J. Jiao, J. Huo, and C. Ma, "An ultrawide band antipodal vivaldi antenna for airborne GPR application," *IEEE Geoscience and Remote Sensing Letters*, vol. 16, no. 10, pp. 1560–1564, Oct. 2019, doi: 10.1109/LGRS.2019.2905013.
- [13] B. Yektakhah, J. Chiu, F. Alsallum, and K. Sarabandi, "Low-profile, low-frequency, UWB antenna for imaging of deeply buried targets," *IEEE Geoscience and Remote Sensing Letters*, vol. 17, no. 7, pp. 1168–1172, Jul. 2020, doi: 10.1109/LGRS.2019.2942007.
- [14] B. Guan, A. Ihamouten, X. Derobert, D. Guilbert, S. Lambot, and G. Villain, "Near-field full-waveform inversion of ground-penetrating radar data to monitor the water front in limestone," *IEEE Journal of Selected Topics in Applied Earth Observations and Remote Sensing*, vol. 10, no. 10, pp. 4328–4336, Oct. 2017, doi: 10.1109/JSTARS.2017.2743215.
- [15] W. Van Verre *et al.*, "Reducing the induction footprint of ultra-wideband antennas for ground-penetrating radar in dual-modality detectors," *IEEE Transactions on Antennas and Propagation*, vol. 69, no. 3, pp. 1293–1301, Mar. 2021, doi: 10.1109/TAP.2020.3026909.
- [16] D. J. Daniels, *Ground penetrating radar*, vol. 1. Wiley, 2005.
- [17] M. I. Skolnik, *Introduction to radar systems*. New York: cGraw Hill Book Co., 1980.
- [18] M. de la V. Pérez Gracia, "Evaluation for applications in archaeology and historical-artistic heritage (in Spanish: radar de subsuelo. Evaluación para aplicaciones en arqueología y en patrimonio histórico-artístico)," Universitat Politècnica de Catalunya, 2001.
- [19] Z. N. Chen, D. Liu, H. Nakano, X. Qing, and T. Zwick, "Handbook of antenna technologies," *Handbook of Antenna Technologies*, vol. 1–4. Springer Singapore, pp. 1–3473, 2016, doi: 10.1007/978-981-4560-44-3.
- [20] T. A. Milligan, *Modern antenna design: second edition*. Wiley, 2005.
- [21] D. M. Pozar, "Microwave engineering, 4th edition," *John Wiley & Sons, Inc.*, pp. 1–756, 2012.
- [22] H. Silva, "Transmission lines and S-parameters applied to metrology (in Spanish: Líneas de transmisión y parámetros S aplicados a la metrología)," *Instituto Nacional de Tecnología Industrial*, 2014, [Online]. Available: <http://www.inti.gov.ar/electronicaeinformatica/metrologiarf>.
- [23] A. Liu and J. Lu, "A UHF deployable log periodic dipole antenna: concept, design, and experiment," *IEEE Transactions on Antennas and Propagation*, vol. 69, no. 1, pp. 538–543, Jan. 2020, doi: 10.1109/TAP.2020.3004986.
- [24] A. Srivastav, P. Nguyen, M. McConnell, K. A. Loparo, and S. Mandal, "A highly digital multi-antenna ground-penetrating radar (GPR) system," *IEEE Transactions on Instrumentation and Measurement*, vol. 69, no. 10, pp. 7422–7436, Oct. 2020, doi: 10.1109/TIM.2020.2984415.
- [25] J. Poikajrvi, K. Peisa, T. Herronen, P. O. Aursand, P. Maijala, and A. Narbro, "GPR in road investigations-equipment tests and quality assurance of new asphalt pavement," *Nondestructive Testing and Evaluation*, vol. 27, no. 3, pp. 293–303, Sep. 2012, doi: 10.1080/10589759.2012.695786.
- [26] "ETTUS USRP B210 SDR," *Ettus Research*. <https://www.ettus.com/all-products/ub210-kit/> (accessed Sep. 08, 2023).
- [27] M. S. Gawade and R. D. Joshi, "GNU radio and USRP B210 based software defined radio for OFDM data transmission," in *2021 IEEE International Conference on Mobile Networks and Wireless Communications, ICMNWC 2021*, Dec. 2021, pp. 1–5, doi: 10.1109/ICMNWC52512.2021.9688506.

BIOGRAPHIES OF AUTHORS



Marco Antonio Becerra-Pérez    is an associate researcher in the technological development of the radio frequency, microwave and optics research group of the Telecommunications Research and Training Institute, Lima, Peru. He is currently a master's student in Mathematical Engineering at the Universidad Nacional de Trujillo and holds a bachelor's degree in Mechatronics Engineering from the same university. His research interests include microwaves, optics, mechatronics design, and robotics. He can be contacted at email: mbecerra@inictel-uni.edu.pe.



Tanith Guerra-Huaranga    is a Bachelor of Telecommunications at the National University of Engineering, Lima, Peru in 2018. Member IEEE, in 2019 to 2020 he was a student representative of SAC Team Peru. His current research interests include RF/MW/mmW devices, antennas, metamaterial radars, and communication system transmitters. She can be contacted at email: tguerrah@uni.pe.



Maria Elisia Armas-Alvarado    is an Electronic Engineer graduated in 2009. Master and Ph.D. in Electrical Engineering from the University of Sao Paulo (Brazil) in 2012 and 2017, respectively. She is currently researcher in the at the National Institute for Research and Training in Telecommunications. Her research areas include microelectronics, microfluidics, optoelectronics, photonics, and materials science. She actively participates in research project especially linked to the design, modeling, and manufacturing of devices. She can be contacted at email: marmas@inictel-uni.edu.pe.



Mark Clemente-Arenas    is a full professor at National University of South Lima UNTELS. He received his Ph.D. from Telecom Paristech in Telecommunications and Electronics. He has a M.Sc. degree on Communicating Objects from the Universite d'Aix Marseille. He also obtained a MEng degree in Microelectronics and Telecommunications from the Polytech Marseille. His B.S. degree is on Electronic Engineering at the Universidad Nacional de San Antonio Abad del Cusco. His research areas include RF/MW/mmW devices, antennas, metamaterials and complex materials for various applications such as 5G, radars, wireless sensors, satellites and EM modeling. He can be contacted at email: mclemente@untels.edu.pe.



Ruth Esther Rubio-Noriega    is the leader of the Telecommunications and Information Technologies Group at the National Institute for Research and Training in Telecommunications and is a lecturer at the National University of Engineering in Lima, Peru. She has a Ph.D. and M.Sc. in Telecommunications and Telematics from the State University of Campinas in Sao Paulo, Brazil, in 2017. Her research areas include integrated photonics, optoelectronic devices, optical interconnects, microwaves for optical devices, applied and computational electromagnetism. She can be contacted at email: rrubio@inictel-uni.edu.pe.